Turkish Journal of Physics

http://journals.tubitak.gov.tr/physics/

Research Article

Turk J Phys
(2019) 43: 67 – 79

doi:10.3906/fiz-1807-62

Lorentz-violating effects in single W boson production at the LHC

Serdar SPOR[1*], **İnanç ŞAHİN**[2]

[1]Department of Physics, Faculty of Arts and Sciences, Zonguldak Bülent Ecevit University, Zonguldak, Turkey
[2]Department of Physics, Faculty of Sciences, Ankara University, Ankara, Turkey

Received: 31.07.2018 • **Accepted/Published Online:** 07.12.2018 • **Final Version:** 22.02.2019

Abstract: We investigate the Lorentz-violating effects of Standard Model Extension (SME) in single W boson production process $pp \to p\gamma p \to pW^- q' X$ at the Large Hadron Collider (LHC). We employ the Weizsacker–Williams approximation for photons emitted from one of the incoming proton beams and consider $\gamma q \to W^- q'$ as a subprocess in the proton-proton collision. The behavior of the differential cross-section for various orientations of the constant background fields is obtained by taking into account longitudinal and transverse polarization states of the final W bosons.

Key words: Lorentz violation, Standard Model Extension, Large Hadron Collider

1. Introduction

The Standard Model (SM) of particle physics and Einstein's general theory of relativity are the most successful theories to date. Lorentz symmetry is involved as a fundamental assumption in both of these theories and the unification of these theories is expected to make an agreement at Planck scale, $m_p \simeq 10^{19}$ GeV, for a unified quantum description of nature. The Planck scale is 10^{15} times larger than the energy achieved at the LHC. Therefore, it is currently not possible to conduct experiments directly on the Planck scale. On the other hand, some suppressed effects emerging from the unified quantum theory at the Planck scale might be observable in highly sensitive low-energy experiments. One such candidate is the violation of the equivalence principle associated with Lorentz symmetry breaking [1–4]. As was discussed in the literature, Lorentz violations can exist in mechanisms of string theory or quantum gravity [5–8]. Any observable signal that may originate from Lorentz violation can be defined via an effective field theory [9]. The Standard Model Extension (SME) is such an effective field theory model, which contains violation of the Lorentz symmetry [2, 9]. The minimal version of SME without gravity offers some useful features: energy-momentum conservation, observer Lorentz invariance, quantization, hermiticity, microcausality, positivity of the energy, gauge invariance, and power counting renormalizability [10]. In recent years, the Lorentz-violating coefficients in the minimal SME have been adopted by experimentalists for reporting sensitivity constraints on Lorentz violation. The minimal SME has been used comprehensively by theorists and experimentalists to search for leading-order signals of Lorentz violation [11, 12]. Lorentz violation can be considered especially as a source of new physics effects [13, 14].

In the context of SME, there are two possible classes of Lorentz transformations, namely the observer and the particle Lorentz transformations. Observer transformations are performed as changes of coordinate systems as in the conventional Lorentz transformations. On the other hand, particle Lorentz transformations are

*Correspondence: serdar.spor@beun.edu.tr

performed on particle fields without changing the observer's frame. Although these two types of transformations are equivalent in most cases, the equivalence does not hold when there is a background field [2, 15]. The main motivation of the SME is that even in the case in which particle Lorentz symmetry is broken, physics can remain invariant under observer Lorentz transformations. This peculiar situation might happen in the presence of constant background fields. For instance, assume that we have a constant background tensor field $b^{\theta\phi}$. Then $b^{\theta\phi}$ transforms as a rank-2 tensor under observer Lorentz transformations, but transforms as 4×4 scalars under particle Lorentz transformations. Consequently, observer Lorentz symmetry remains invariant, but particle Lorentz symmetry is broken.

In this paper, we are interested in the subprocess $\gamma q \to W^- q'$ in photon-proton collisions at the Large Hadron Collider (LHC) in the presence of a constant antisymmetric tensor background field $b^{\theta\phi}$. The existence of this background field throughout the spacetime implies spontaneous Lorentz violation, and we search for its phenomenological implications. In this respect, we investigate the deviations of SM predictions in the subprocess $\gamma q \to W^- q'$, which arise from Lorentz violating effects in the $WW\gamma$ vertex. Thus, we will focus on the new physics effects in the SME approach. The process $\gamma q \to W^- q'$ takes part as a subprocess in $p\,p \to p\,\gamma\,p \to p\,W^-\,q'\,X$ in the proton-proton collision. Here q and q' represent the quark fields and X represents the proton remnants after deep inelastic scattering. We consider the following eight independent subprocesses of the main process and sum up the contributions from each subprocess.

$$\begin{aligned}
&\text{(i)}\quad \gamma\, d \to W^-\, u && \text{(v)}\quad \gamma\, \overline{u} \to W^-\, \overline{d}\\
&\text{(ii)}\quad \gamma\, d \to W^-\, c && \text{(vi)}\quad \gamma\, \overline{u} \to W^-\, \overline{s}\\
&\text{(iii)}\quad \gamma\, s \to W^-\, u && \text{(vii)}\quad \gamma\, \overline{c} \to W^-\, \overline{d}\\
&\text{(iv)}\quad \gamma\, s \to W^-\, c && \text{(viii)}\quad \gamma\, \overline{c} \to W^-\, \overline{s}
\end{aligned} \tag{1.1}$$

The other subprocesses are restricted due to the smallness of the CKM matrix elements. Hence, they are neglected throughout our calculations. We have also neglected subprocesses that include initial state b and t quarks. This assumption is reasonable, since the quark distributions for b and t quarks give tiny probabilities with respect to other quarks.

The photon-induced process $p\,p \to p\,\gamma\,p \to p\,W^-\,q'\,X$ takes place at the LHC via Weizsacker–Williams photons scattered from one of the initial protons. Since the virtuality of these Weizsacker–Williams photons is very low, a proton does not disassociate into partons when it emits a Weizsacker–Williams photon [16, 17]. Consequently, such a proton remains intact and can be detected by the detectors. On the other hand, these intact protons cannot be detected by central detectors. Special detectors called very forward detectors (VFDs) are needed to detect such proton beams. The LHC is planned to be equipped with VFDs, which can detect intact protons [18–20]. An important parameter that characterizes VFDs is the momentum fraction loss ξ of the photon-emitting proton. The range of this parameter determines proton detection acceptance of VFDs. For a realistic value we will consider a forward detector acceptance range of $0.015 < \xi < 0.15$ [18–20].

New physics searches through photon-photon and photon-proton processes at the LHC are widespread in the literature. These studies cover both experimental and phenomenological papers. Some representative experimental ones are given in [21–27] and phenomenological ones are given in [28–58]. On the other hand, as far as we know, SME and Lorentz symmetry violation has not been studied in photon-photon and photon-proton processes at the LHC. Our paper is the first to investigate Lorentz-violating effects in a photon-proton process at the LHC.

2. The cross section of $\gamma q \to W^- q'$

The subprocess $\gamma q \to W^- q'$ is described by three tree-level Feynman diagrams given in Figure 1. In this paper we will consider a minimal SME scenario and assume that Lorentz-violating effects modify the $WW\gamma$ vertex. As in some papers in the literature (for example, see [13, 14]), we neglect other contributions that may come from SME (for instance, contributions from rank-4 tensors) and assume that the Lagrangian for the $WW\gamma$ vertex is given by

$$\mathcal{L}_{SME} = \frac{ig_e}{2} b^{\theta\phi} (W^-_{\theta\nu} W^+_{\phi\lambda} F^{\nu\lambda} + W^+_{\theta\nu} W^{-\nu\lambda} F_{\phi\lambda} + W^-_{\phi\lambda} W^{+\nu\lambda} F_{\theta\nu}), \tag{2.1}$$

where $b^{\theta\phi}$ is the constant background tensor, which is antisymmetric and has dimension of inverse mass square. The field strength tensors for vector fields $W_{\mu\nu}$ and $F_{\mu\nu}$ can be written as follows:

$$W_{\mu\nu} = \partial_\mu W_\nu - \partial_\nu W_\mu, \tag{2.2}$$

$$F_{\mu\nu} = \partial_\mu A_\nu - \partial_\nu A_\mu, \tag{2.3}$$

where W_μ and A_μ are the W boson and photon fields, respectively.

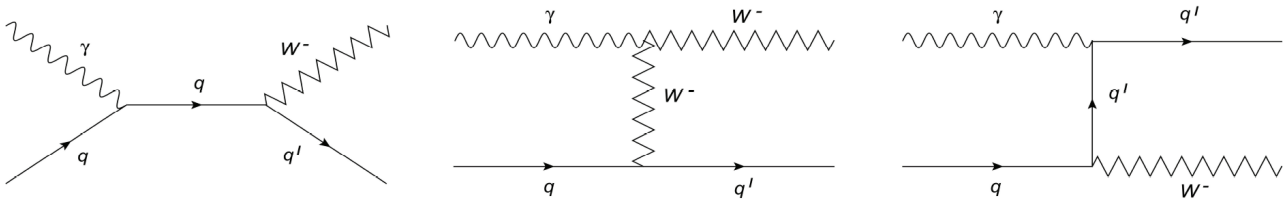

Figure 1. Tree-level Feynman diagrams for the process $\gamma q \to W^- q'$.

The anomalous $WW\gamma$ vertex function obtained from the SME Lagrangian in Eq. (2.1) is given by

$$\Gamma_{\mu\nu\lambda}(k_1, k_2, k_3) = \frac{ig_e}{2} b^{\theta\phi} \Gamma_{\theta\phi\mu\nu\lambda}, \tag{2.4}$$

where

$$\begin{aligned}
\Gamma_{\theta\phi\mu\nu\lambda} = {} & k_{1\nu} k_{2\phi} \left(k_{3\theta} g_{\mu\lambda} - k_{3\mu} g_{\theta\lambda}\right) + k_{1\theta} k_{2\mu} \left(k_{3\nu} g_{\phi\lambda} - k_{3\phi} g_{\nu\lambda}\right) + k_{1\lambda} k_{3\theta} \left(k_{2\mu} g_{\phi\nu} - k_{2\phi} g_{\mu\nu}\right) \\
& + k_{1\phi} k_{3\mu} \left(k_{2\theta} g_{\lambda\nu} - k_{2\lambda} g_{\theta\nu}\right) + k_{2\lambda} k_{3\phi} \left(k_{1\theta} g_{\mu\nu} - k_{1\nu} g_{\mu\theta}\right) + k_{2\theta} k_{3\nu} \left(k_{1\lambda} g_{\mu\phi} - k_{1\phi} g_{\mu\lambda}\right) \\
& + \left(k_1 \cdot k_2\right) \left(k_{3\mu} g_{\phi\nu} g_{\theta\lambda} - k_{3\theta} g_{\phi\nu} g_{\mu\lambda} + k_{3\phi} g_{\mu\theta} g_{\nu\lambda} - k_{3\nu} g_{\mu\theta} g_{\phi\lambda}\right) \\
& + \left(k_1 \cdot k_3\right) \left(k_{2\lambda} g_{\theta\nu} g_{\mu\phi} - k_{2\theta} g_{\mu\phi} g_{\lambda\nu} + k_{2\phi} g_{\mu\nu} g_{\theta\lambda} - k_{2\mu} g_{\phi\nu} g_{\theta\lambda}\right) \\
& + \left(k_2 \cdot k_3\right) \left(k_{1\nu} g_{\mu\theta} g_{\phi\lambda} - k_{1\lambda} g_{\mu\phi} g_{\theta\nu} + k_{1\phi} g_{\theta\nu} g_{\mu\lambda} - k_{1\theta} g_{\mu\nu} g_{\phi\lambda}\right).
\end{aligned} \tag{2.5}$$

Here, k_1 represents the momentum of the photon and k_2 and k_3 represent the momenta of W bosons. Since the background tensor $b^{\theta\phi}$ is antisymmetric, it contains 6 independent parameters. These independent parameters can be parametrized by means of three-vectors $e^i \equiv b^{0i}\Lambda^2$ and $b^i \equiv (1/2)\epsilon^{ijk} b^{jk} \Lambda^2$, where $i, j, k = 1, 2, 3$ and Λ represents the new physics energy scale [59]. The three-vectors $\vec{e}$ and $\vec{b}$ are called electric-like and magnetic-like, respectively, due to the analogy between $b^{\theta\phi}$ and electromagnetic field strength tensor $F^{\theta\phi}$. We

decompose $\vec{e}$ and $\vec{b}$ into parallel e_p (b_p) and perpendicular e_y (b_y) components with respect to the collision plane, which is assumed to be the $x-z$ plane. Then these vectors can be written as $\vec{e}=(e_p\sin\psi, e_y, e_p\cos\psi)$ and $\vec{b}=(b_p\sin\beta, b_y, b_p\cos\beta)$. For details, see Figure 2. Contraction of $b^{\theta\phi}$ with arbitrary four-vectors a_θ and c_ϕ is given by the following identity:

$$a_\theta c_\phi b^{\theta\phi} = \frac{1}{\Lambda^2}[\vec{b}\cdot(\vec{a}\times\vec{c}) + c_0\,\vec{e}\cdot\vec{a} - a_0\,\vec{e}\cdot\vec{c}]. \tag{2.6}$$

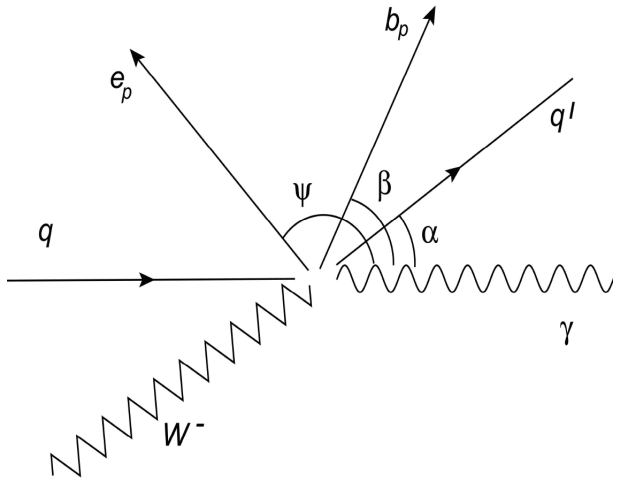

Figure 2. Scattering process $\gamma q \to W^- q'$ in the center-of-momentum frame. The orientations of vectors $\vec{e}$ and $\vec{b}$ are shown in the figure.

The scattering amplitude for the subprocess $\gamma q \to W^- q'$ is calculated by using the helicity amplitude method. The polarization vectors for photon $A^\mu(k_1)$ and W boson $W^\nu(k_2)$ fields can be written as follows [60]:

$$\epsilon^\mu(k_1,\varphi_\gamma) = \frac{1}{\sqrt{2}}\,(0,\,-\varphi_\gamma,\,i,\,0)\,, \tag{2.7}$$

$$\epsilon^\nu(k_2,\varphi_w) = \frac{1}{\sqrt{2}}\,(0,\,\varphi_w\cos\,\alpha,\,-i,\,-\varphi_w\sin\,\alpha)\,, \tag{2.8}$$

$$\epsilon^\nu(k_2,0) = \frac{1}{2m_w\sqrt{s}}\left(s-m_w^2,\,-(s+m_w^2)\sin\,\alpha,\,0,\,-(s+m_w^2)\cos\,\alpha\right), \tag{2.9}$$

where φ_γ and φ_w indicate transverse polarization states for the photon and W^- boson and can take either +1 or –1. Here, m_w is the mass of the W boson, s is the Mandelstam parameter, and α is the scattering angle in the center-of-momentum frame (see Figure 2). Longitudinal polarization state of the W boson is given in Eq. (2.9) and sometimes represented by $\varphi_w = 0$. The helicity amplitudes of SME can be written as a sum of SM and new physics (NW) amplitudes:

$$M^{SME}_{\varphi_\gamma,\,\varphi_w} = M^{SM}_{\varphi_\gamma,\,\varphi_w} + M^{NW}_{\varphi_\gamma,\,\varphi_w}. \tag{2.10}$$

Since the initial state photons in $\gamma q \to W^- q'$ are emitted from unpolarized proton beams, these Weizsacker–Williams photons should also be unpolarized. Therefore, we consider the case in which initial state photons

are unpolarized whereas final state W bosons are polarized. To get a squared amplitude for unpolarized initial photons but polarized final W, we sum squared amplitudes for $\varphi_\gamma = +1$ and $\varphi_\gamma = -1$:

$$|M_{unpol,\varphi_w}|^2 = |M_{+1,\varphi_w}|^2 + |M_{-1,\varphi_w}|^2. \tag{2.11}$$

Final state W boson polarization can be determined by the angular distribution of its decay products. However, it is experimentally difficult to distinguish $\varphi_w = +1$ and $\varphi_w = -1$ cases. Hence, we consider only transverse and longitudinal polarizations states of the final W boson. Squared amplitudes for transverse (tr) and longitudinal (lo) polarizations are defined as follows:

$$|M_{unpol,\,tr}|^2 = \quad |M_{unpol,\,+1}|^2 + |M_{unpol,\,-1}|^2, \tag{2.12}$$

$$|M_{unpol,\,lo}|^2 = \quad |M_{unpol,\,0}|^2. \tag{2.13}$$

The differential cross-section of the subprocess is then obtained from the following well-known formula:

$$\left(\frac{d\sigma_{unpol,\,tr(lo)}}{d\Omega}\right) = \frac{s - m_w^2}{64\pi^2 s^2}\,|M_{unpol,\,tr(lo)}|^2. \tag{2.14}$$

3. Weizsacker–Williams approximation and the cross-section for $\mathbf{p\,p \to p\,\gamma\,p \to p\,W^-\,q'\,X}$

The cross-section of the main process $p\,p \to p\,\gamma\,p \to p\,W^-\,q'\,X$ is obtained by integrating the cross-section of $\gamma q \to W^- q'$ over initial photon and quark distributions:

$$\begin{aligned}\sigma\left(p\,p \to p\,\gamma\,p \to p\,W^-\,q\,X\right) = \int_{Q^2_{min}}^{Q^2_{max}} dQ^2 \int_{x_{1\,min}}^{x_{1\,max}} dx_1 \int_{x_{2\,min}}^{x_{2\,max}} dx_2 \\ \times \left(\frac{dN_\gamma}{dx_1 dQ^2}\right)\left(\frac{dN_q}{dx_2}\right)\hat{\sigma}_{\gamma q \to W q'}\left(\hat{s}\right),\end{aligned} \tag{3.1}$$

where Q^2 and x_1 are the virtuality and energy fraction of initial photons and x_2 is the momentum fraction of the proton's momentum carried by the quark. $\frac{dN_q}{dx_2}$ is the quark distribution function of the proton. In our calculations parton distribution functions of Martin, Stirling, Thorne, and Watt [61] have been used. $\frac{dN_\gamma}{dx_1 dQ^2}$ is the photon distribution function, which describes a photon spectrum of virtuality Q^2 and energy fraction x_1. When we employ the Weizsacker–Williams approximation, the equivalent photon distribution for equivalent photons emitted from the incoming proton beam can be written by the following analytical formula [62–64]:

$$\frac{dN_\gamma}{dE_\gamma dQ^2} = \frac{\alpha}{\pi}\frac{1}{E_\gamma Q^2}\left[\left(1 - \frac{E_\gamma}{E}\right)\left(1 - \frac{Q^2_{min}}{Q^2}\right)F_E + \frac{E_\gamma^2}{2E^2}F_M\right], \tag{3.2}$$

where

$$Q^2_{min} = \frac{m_p^2 E_\gamma^2}{E\left(E - E_\gamma\right)}, \qquad F_E = \frac{4m_p^2 G_E^2 + Q^2 G_M^2}{4m_p^2 + Q^2}, \tag{3.3}$$

$$G_E^2 = \frac{G_M^2}{\mu_p^2} = \left(1 + \frac{Q^2}{Q_0^2}\right)^{-4}, \qquad F_M = G_M^2, \qquad Q_0^2 = 0.71\,GeV^2. \tag{3.4}$$

Here, E is the energy of proton beam, m_p is the mass of the proton, and $\mu_p^2 = 7.78$ is the magnetic moment of the proton. F_E and F_M are functions of the electric and magnetic form factors.

We analyze the effects of SME by considering two different scenarios. In the first scenario we assume that $\vec{e} = 0$ but $\vec{b} \neq 0$ $(b_p = b_y = 1)$. Therefore, in this scenario we have one free parameter, which is the angle β (see Figure 2). In the second scenario we assume that $\vec{e} \neq 0$ $(e_p = e_y = 1)$ but $\vec{b} = 0$. We then have a free parameter ψ. In Figure 3, we plot SM differential cross-sections for the main process $pp \to p\gamma p \to pW^- q' X$ for longitudinally, transversely, and unpolarized final W bosons. In all calculations in this work we assume that the center-of-mass energy of the proton-proton system is 14 TeV. In Figures 4–6, we present the differential cross-section as a function of the cosine of the β parameter, which specifies the orientation of the magnetic-like vector in scenario 1. We consider $\alpha = 30°$, $60°$, $90°$, $120°$, and $150°$ values of the scattering angle. In all plots the new physics energy scale is taken to be $\Lambda = 500$ GeV. We observe from these figures that the behaviors of the differential cross-sections in transversely polarized and unpolarized cases are very similar to each other. On the other hand, the longitudinally polarized cross-section exhibits a different behavior. In Figures 7–9, we present the differential cross-section as a function of the cosine of the ψ parameter, which specifies the orientation of the electric-like vector in scenario 2. We consider $\alpha = 30°$, $60°$, $90°$, $120°$, and $150°$ values of the scattering angle. Again, in all plots, the new physics energy scale is taken to be $\Lambda = 500$ GeV. We observe from these figures that as in the case of scenario 1 the behaviors of the differential cross-sections in transversely polarized and unpolarized cases are very similar to each other. However, the longitudinally polarized cross-section exhibits a different behavior. Therefore, we conclude that in both of the scenarios, the comparison of longitudinally and transversely polarized cross-sections is useful in probing Lorentz-violating effects of SME in the process $pp \to p\gamma p \to pW^- q' X$. We also observe from Figures 4–9 that the behaviors of the polarized differential cross-sections are different in different scenarios.

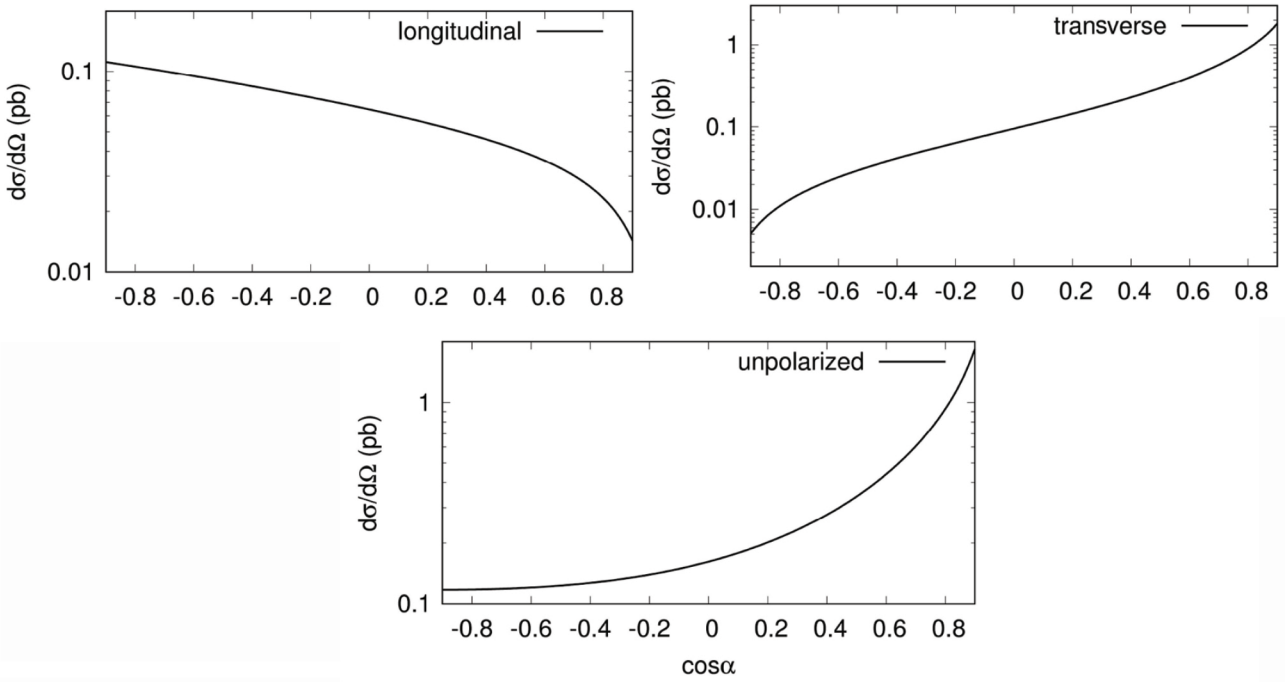

Figure 3. Differential cross-section of $pp \to p\gamma p \to pW^- q' X$ as a function of scattering angle $cos\alpha$ for the SM. Figures from top to bottom show longitudinal polarization, transverse polarization, and unpolarized cases, respectively.

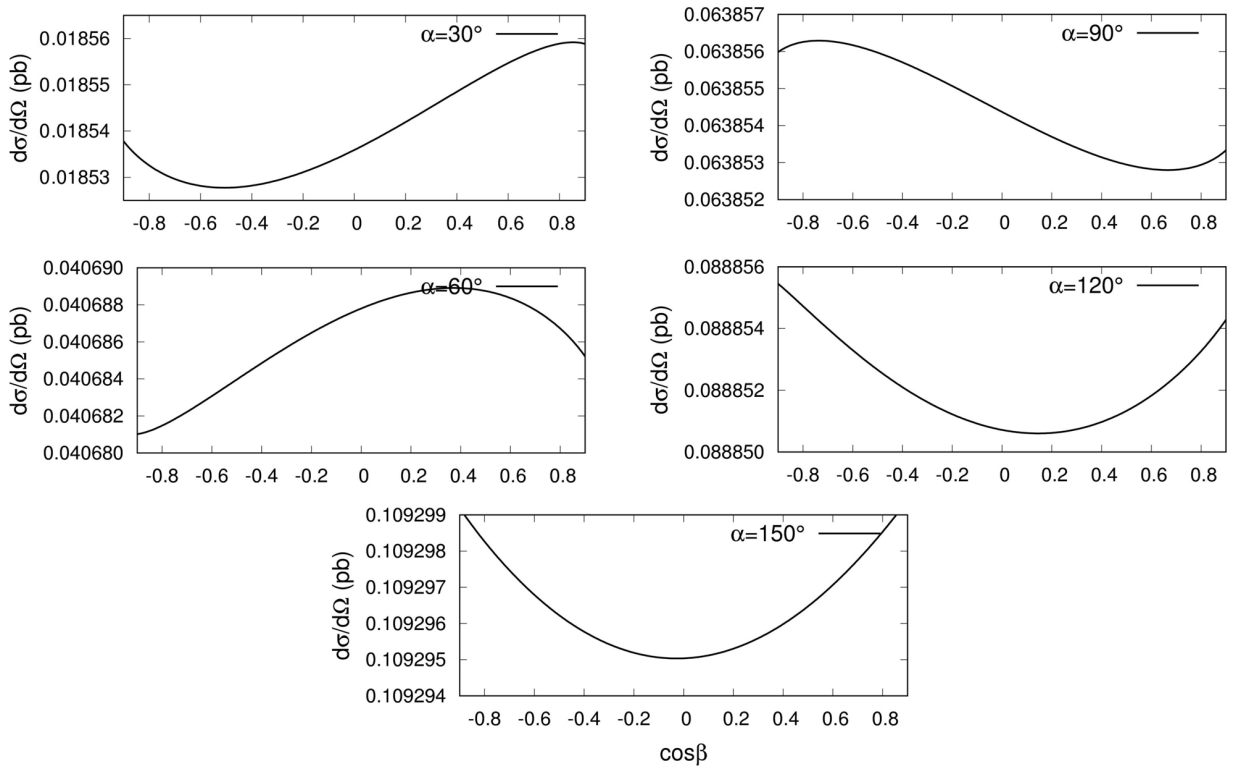

Figure 4. Differential cross-section of $pp \rightarrow p\gamma p \rightarrow pW^- q' X$ as a function of $cos\beta$ in scenario 1. Figures from top to bottom show the following values of the scattering angle: $\alpha = 30^\circ$, 60°, 90°, 120°, and 150°. We consider the longitudinal polarization case.

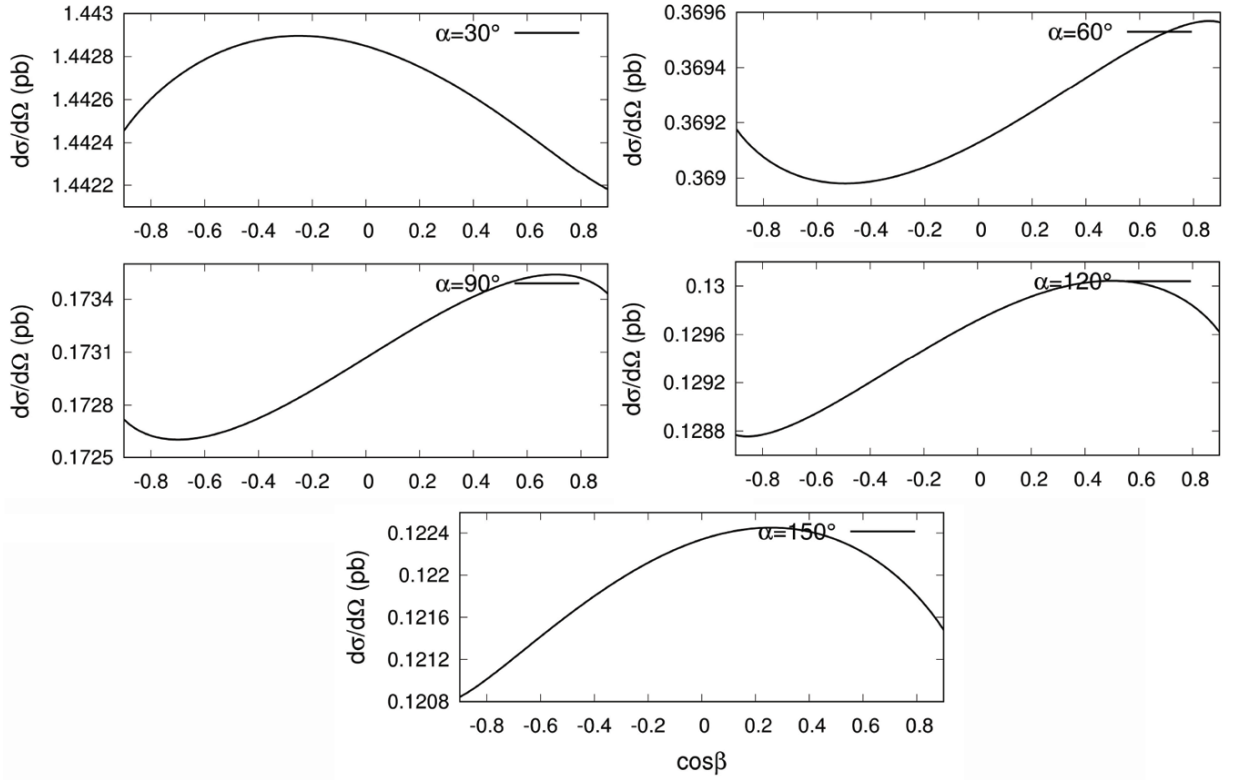

Figure 5. The same as Figure 4 but for transverse polarization case.

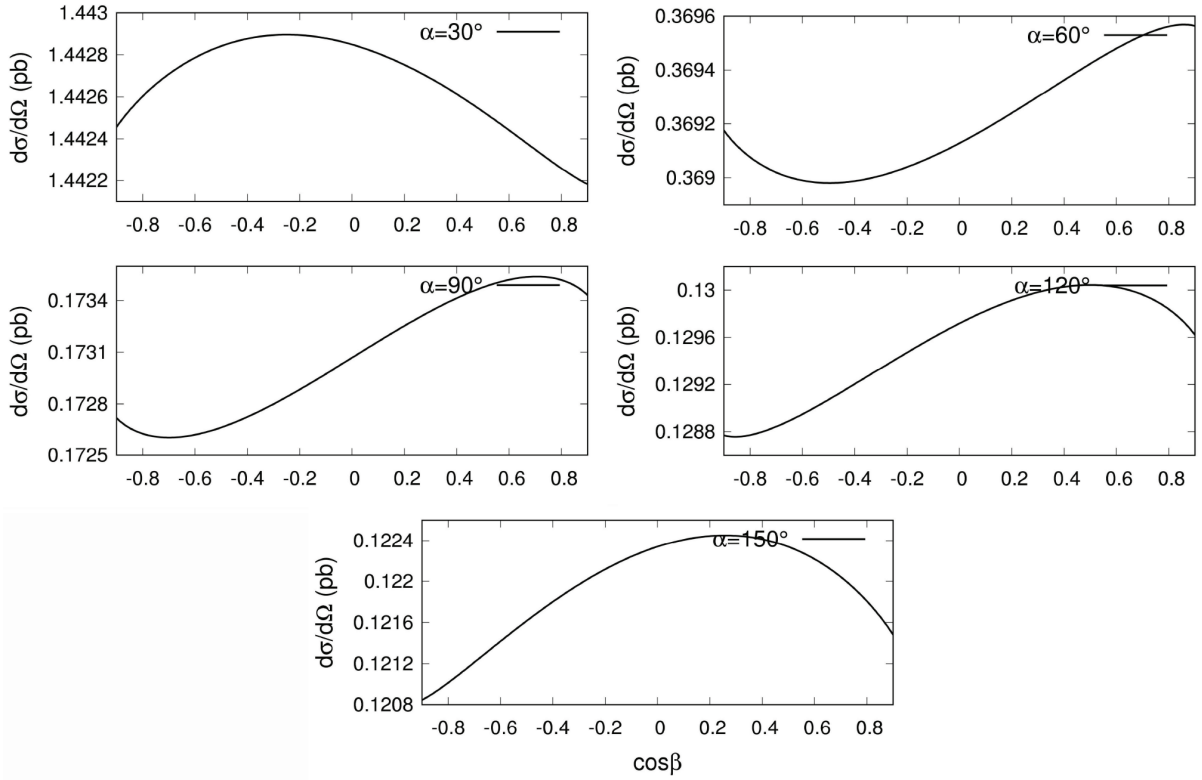

Figure 6. The same as Figure 4 but for unpolarized case.

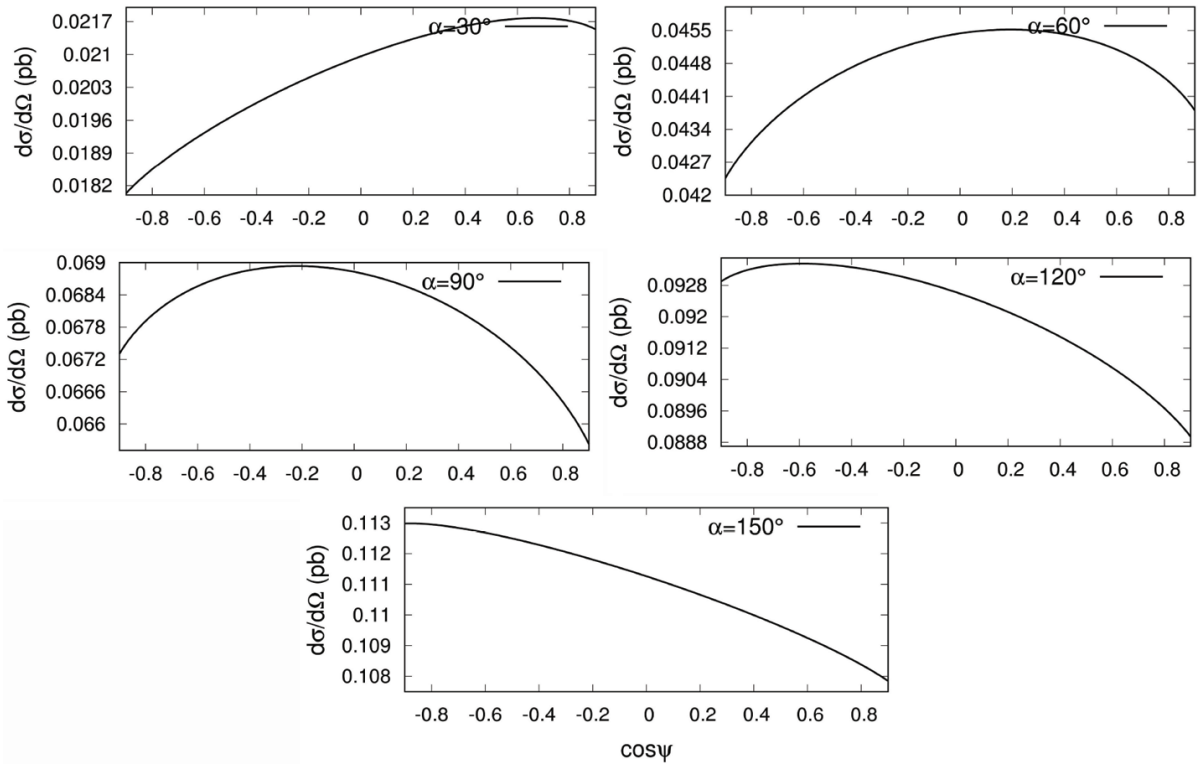

Figure 7. Differential cross-section of $pp \to p\gamma p \to pW^- q' X$ as a function of $cos\psi$ in scenario 2. Figures from top to bottom show the following values of the scattering angle: $\alpha = 30^\circ$, 60°, 90°, 120°, and 150°. We consider the longitudinal polarization case.

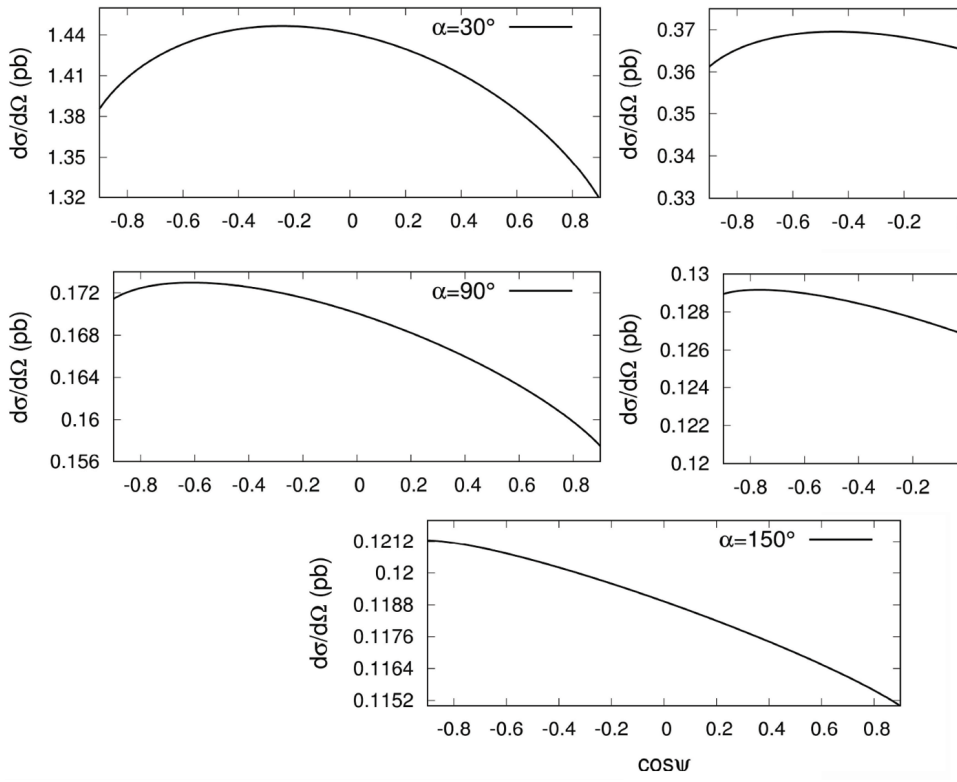

Figure 8. The same as Figure 7 but for transverse polarization case.

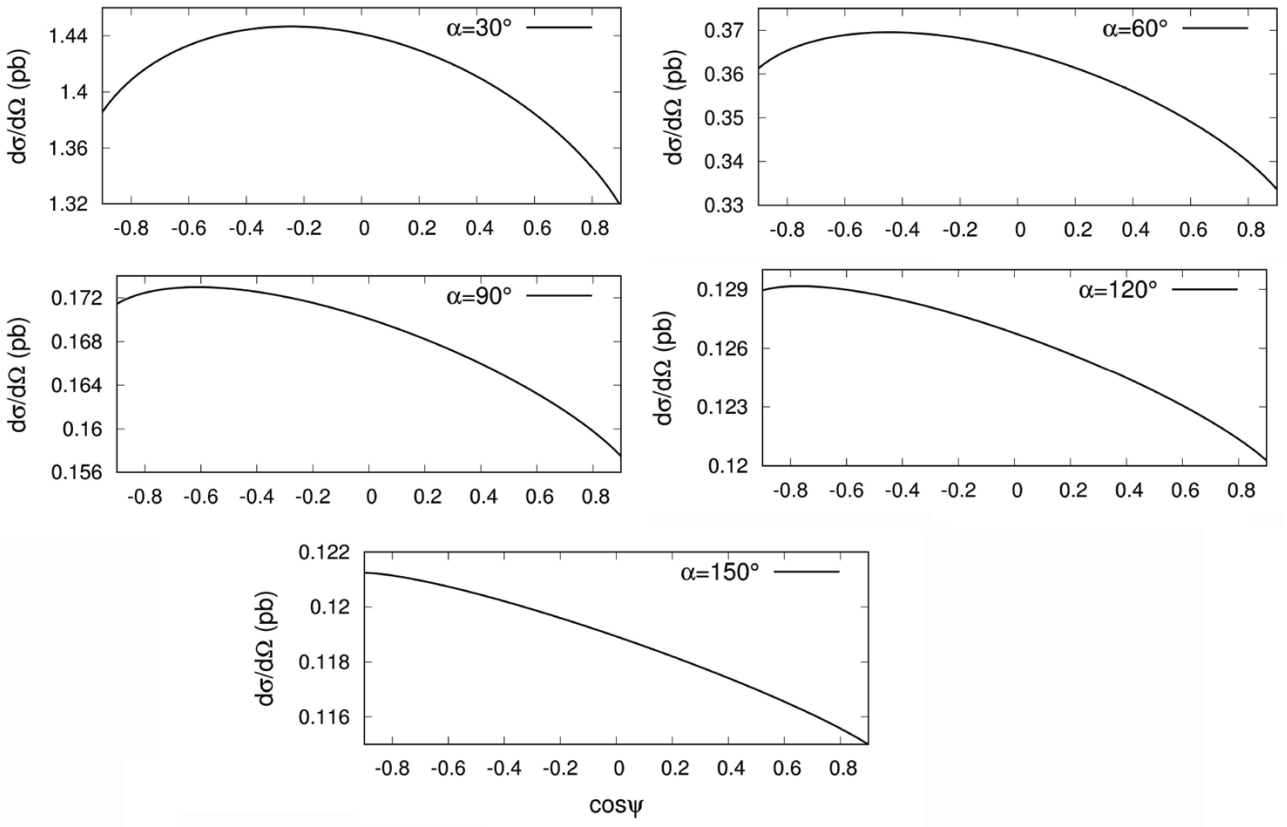

Figure 9. The same as Figure 7 but for unpolarized case.

In a real experiment the collision plane (the plane spanned by the momenta of the incoming photon and outgoing W boson) varies at each collision. On the other hand, $\vec{e}$ and $\vec{b}$ are constant background vectors and although they are fixed under particle Lorentz transformations we do not know what their real orientations are. The best thing we can do is to examine the effects of these background vectors on the cross-section under some simplifying assumptions. For this purpose we have assumed two different scenarios, and each has one free parameter that defines the orientation of electric-like (scenario 2) and magnetic-like (scenario 1) vectors in the collision plane. In Figures 10–13, we perform a different analysis. We assume that only one type of (electric-like or magnetic-like) vector is nonzero, but different from previous scenarios, we consider randomly chosen orientations for this nonzero vector. Each time we pick a random orientation of the vector, which is uniformly distributed on a sphere, and we calculate the corresponding differential cross-section. The results of these calculations are given in Figure 10 and Figure 11 for $\vec{e}=0$ with $\vec{b}$ chosen randomly and in Figure 12 and Figure 13 for $\vec{b}=0$ with $\vec{e}$ chosen randomly.

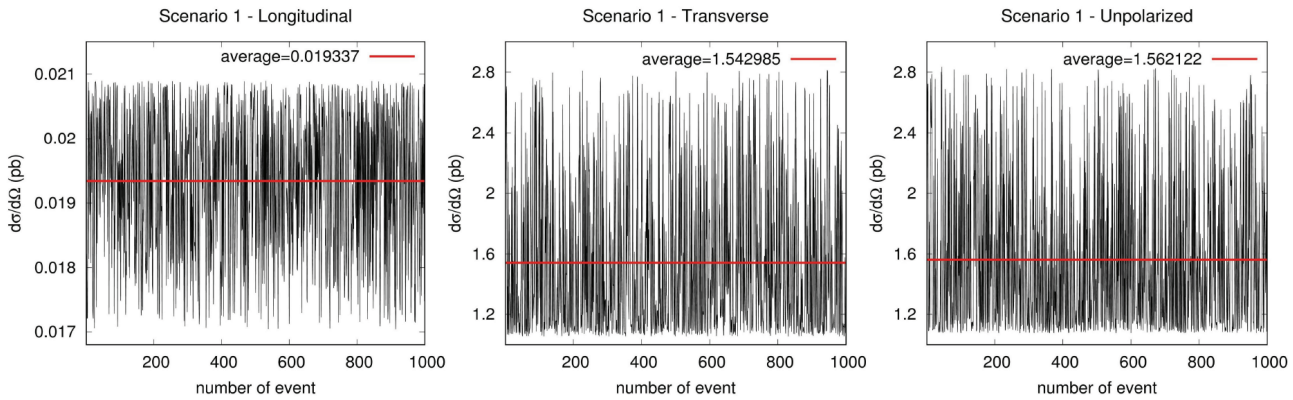

Figure 10. Differential cross-sections for randomly chosen orientations of magnetic-like vector $\vec{b}$. The horizontal axis shows random numbers generated by a random generator. The electric-like vector is taken to be zero ($\vec{e}=0$). Figure on the left shows the differential cross-section for longitudinal polarization state of the W boson. Middle figure shows transverse polarization and right figure shows unpolarized cases. The scattering angle is $\alpha=30^{\circ}$ and $\Lambda=200$ GeV.

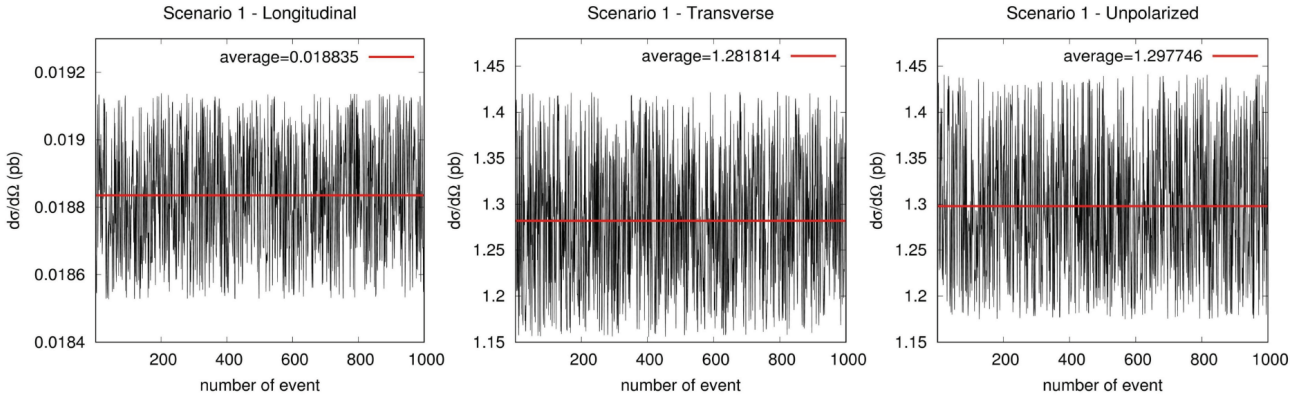

Figure 11. The same as Figure 10 but for $\Lambda=500$ GeV.

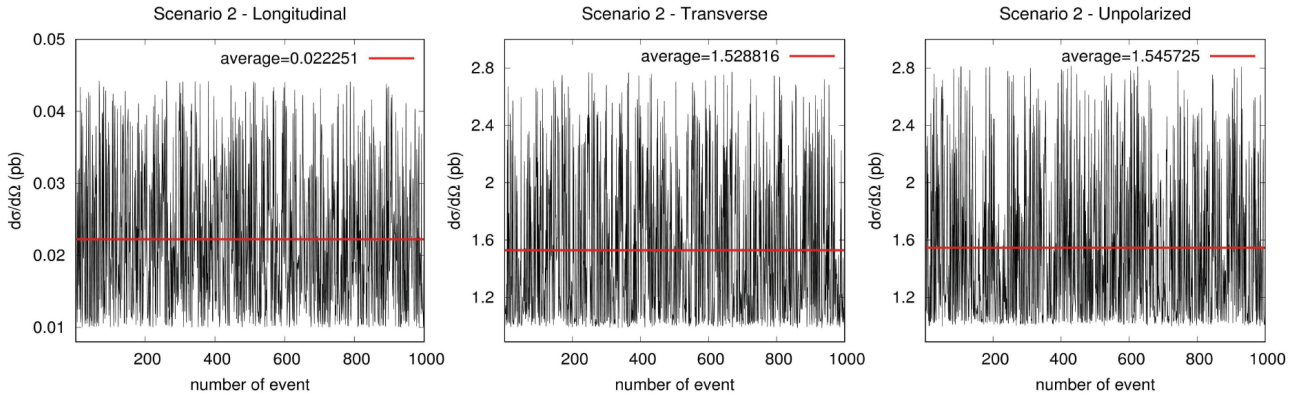

Figure 12. Differential cross-sections for randomly chosen orientations of electric-like vector $\vec{e}$. The horizontal axis shows random numbers generated by a random generator. The magnetic-like vector is taken to be zero ($\vec{b} = 0$). Figure on the left shows the differential cross-section for longitudinal polarization state of the W boson. Middle figure shows transverse polarization and right figure shows unpolarized cases. The scattering angle is $\alpha = 30^{\circ}$ and $\Lambda = 200$ GeV.

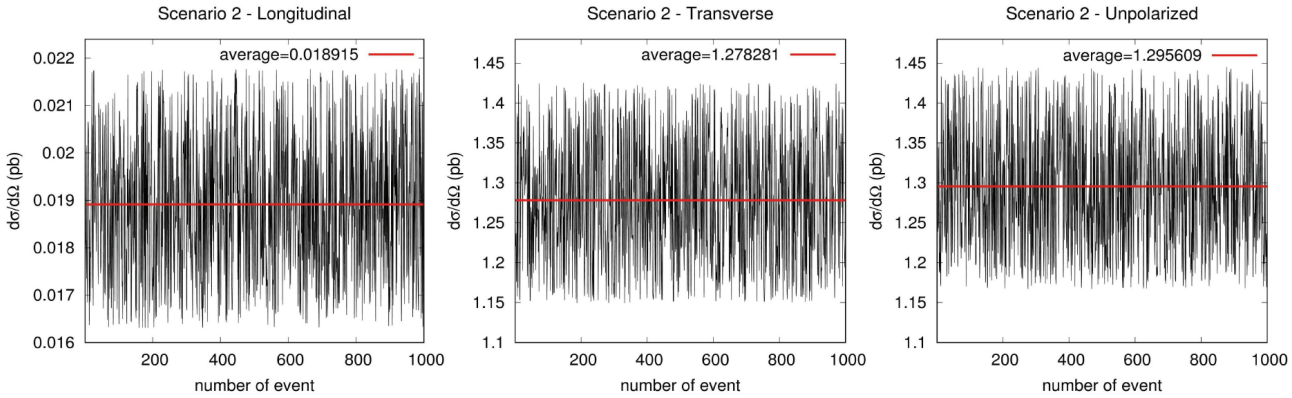

Figure 13. The same as Figure 12 but for $\Lambda = 500$ GeV.

4. Conclusion

We have investigated the Lorentz-violating effects of SME in single W boson production $pp \to p\gamma p \to pW^- q' X$ at the LHC. We have shown that the differential cross-section is sensitive to electric and magnetic-like vectors $\vec{e}$ and $\vec{b}$, which define the background tensor field. We have also shown that the behavior of the differential cross-section depends on the polarization state of final W bosons. Therefore, in a real experiment both the angular distribution of final W bosons and their polarization will provide us essential data to analyze possible new physics contributions from SME.

References

[1] Kostelecky, V. A. *Phys. Rev. D* **2004**, *69*, 105009.

[2] Colladay, D.; Kostelecky, V. A. *Phys. Rev. D* **1998**, *58*, 116002.

[3] Coleman, S. R.; Glashow, S. L. *Phys. Rev. D* **1999**, *59*, 116008.

[4] Coleman, S. R.; Glashow, S. L. *Phys. Lett. B* **1997**, *405*, 249-252.

[5] Kostelecky, V. A.; Samuel, S. *Phys. Rev. D* **1989**, *40*, 1886-1903.

[6] Kostelecky, V. A.; Samuel, S. *Phys. Rev. D* **1989**, *39*, 683-685.

[7] Kostelecky, V. A.; Potting, R. *Nucl. Phys. B* **1991**, *359*, 545-570.

[8] Kostelecky, V. A.; Samuel, S. *Phys. Rev. Lett.* **1989**, *63*, 224-227.

[9] Kostelecky, V. A.; Potting, R. *Phys. Rev. D* **1995**, *51*, 3923-3935.

[10] Colladay, D.; McDonald, P. *Phys. Rev. D* **2004**, *70*, 125007.

[11] Bluhm, R. *Lect. Notes Phys.* **2006**, *702*, 191-226.

[12] Bluhm, R. In *The Springer Handbook of Spacetime;* Ashtekar, A.; Petkov, V., Eds. Springer-Verlag: Berlin, Germany, 2014, pp. 485-507.

[13] Aranda, J. I.; Ramírez-Zavaleta, F.; Rosete, D. A.; Tlachino, F. J.; Toscano, J. J.; Tututi, E. S. *J. Phys. G* **2014**, *41*, 055003.

[14] Aranda, J. I.; Ramírez-Zavaleta, F.; Tlachino, F. J.; Toscano, J. J.; Tututi, E. S. *Int. J. Mod. Phys. A* **2014**, *29*, 1450180.

[15] Colladay, D.; Kostelecky, V. A. *Phys. Rev. D* **1997**, *55*, 6760-6774.

[16] Rouby, X. PhD, Universite Catholique de Louvain, Louvain-la-Neuve, Belgium, 2008.

[17] Schul, N. PhD, Universite Catholique de Louvain, Louvain-la-Neuve, Belgium, 2011.

[18] Allport, P.; Nessi, M. *Letter of Intent for the Phase-I Upgrade of the ATLAS Experiment, CERN-LHCC-2011-012*; CERN: Geneva, Switzerland, 2011.

[19] Albrow, M.; Arneodo, M.; Avati, V.; Baechler, J.; Cartiglia, N.; Deile, M.; Gallinaro, M.; Hollar, J.; Lo Vetere, M.; Oesterberg, K. et al. *CMS-TOTEM Precision Proton Spectrometer, CERN-LHCC-2014-021*; CERN: Geneva, Switzerland, 2014.

[20] Tasevsky, M. *AIP Conf. Proc.* **2015**, *1654*, 090001.

[21] Chatrchyan, S.; Khachatryan, V.; Sirunyan, A. M.; Tumasyan, A.; Adam, W.; Bergauer, T.; Dragicevic, M.; Erö, J.; Fabjan, C.; Friedl, M.; et al. *J. High Energy Phys.* **2012**, *01*, 052.

[22] Chatrchyan, S.; Khachatryan, V.; Sirunyan, A. M.; Tumasyan, A.; Adam, W.; Bergauer, T.; Dragicevic, M.; Erö, J.; Fabjan, C.; Friedl, M. et al. *J. High Energy Phys.* **2012**, *11*, 080.

[23] Chatrchyan, S.; Khachatryan, V.; Sirunyan, A. M.; Tumasyan, A.; Adam, W.; Bergauer, T.; Dragicevic, M.; Erö, J.; Fabjan, C.; Friedl, M. et al. *J. High Energy Phys.* **2013**, *07*, 116.

[24] Khachatryan, V.; Sirunyan, A. M.; Tumasyan, A.; Adam, W.; Asilar, E.; Bergauer, T.; Brandstetter, J.; Brondolin, E.; Dragicevic, M.; Erö, J. et al. *J. High Energy Phys.* **2016**, *08*, 119.

[25] Aaboud, M.; Aad, G.; Abbott, B.; Abdallah, J.; Abdinov, O.; Abeloos, B.; Aben, R.; AbouZeid, O. S.; Abraham, N. L.; Abramowicz, H. et al. *Phys. Rev. D* **2016**, *94*, 032011.

[26] Baldenegro, C.; Fichet, S.; Von Gersdorff, G.; Royon, C. *J. High Energy Phys.* **2018**, *06*, 131.

[27] Sirunyan, A. M.; Tumasyan, A.; Adam, W.; Ambrogi, F.; Asilar, E.; Bergauer, T.; Brandstetter, J.; Brondolin, E.; Dragicevic, M.; Erö, J. et al. *J. High Energy Phys.* **2018**, *07*, 153.

[28] Ginzburg, I. F.; Schiller, A. *Phys. Rev. D* **1999**, *60*, 075016.

[29] Khoze, V. A.; Martin, A. D.; Ryskin, M. G. *Eur. Phys. J. C* **2002**, *23*, 311-327.

[30] Schul, N.; Piotrzkowski, K. *Nucl. Phys. B Proc. Suppl.* **2008**, *179-180*, 289-297.

[31] Kepka, O.; Royon, C. *Phys. Rev. D* **2008**, *78*, 073005.

[32] Şahin, İ.; İnan, S. C. *J. High Energy Phys.* **2009**, *09*, 069.

[33] Dougall, T.; Wick, S. D. *Eur. Phys. J. A* **2009**, *39*, 213-217.

[34] Chaichian, M.; Hoyer, P.; Huitu, K.; Khoze, V. A.; Pilkington, A. D. *J. High Energy Phys.* **2009**, *05*, 011.

[35] Chapon, E.; Royon, C.; Kepka, O. *Phys. Rev. D* **2010**, *81*, 074003.

[36] Piotrzkowski, K.; Schul, N. *AIP Conf. Proc.* **2010**, *1200*, 434-437.

[37] İnan, S. C. *Phys. Rev. D* **2010**, *81*, 115002.

[38] Atağ, S.; Billur, A. A. *J. High Energy Phys.* **2010**, *11*, 060.

[39] Goncalves, V. P.; Sauter, W. K. *Phys. Rev. D* **2010**, *82*, 056009.

[40] İnan, S. C.; Billur, A. A. *Phys. Rev. D* **2011**, *84*, 095002.

[41] Şahin, İ.; Billur, A. A. *Phys. Rev. D* **2011**, *83*, 035011.

[42] Şahin, İ.; Köksal, M. *J. High Energy Phys.* **2011**, *03*, 100.

[43] Gupta, R. S. *Phys. Rev. D* **2012**, *85*, 014006.

[44] Epele, L. N.; Fanchiotti, H.; Canal, C. A. G.; Mitsou, V. A.; Vento, V. *Eur. Phys. J. Plus* **2012**, *127*, 60.

[45] Şahin, B.; Billur, A. A. *Phys. Rev. D* **2012**, *86*, 074026.

[46] Şahin, İ.; Billur, A. A.; İnan, S. C.; Şahin, B.; Köksal, M.; Tektas, P.; Alici, E.; Yildirim, R. *Phys. Rev. D* **2013**, *88*, 095016.

[47] Köksal, M.; İnan, S. C. *Adv. High Energy Phys.* **2014**, *2014*, 935840.

[48] Sun, H.; Yue, C. X. *Eur. Phys. J. C* **2014**, *74*, 2823.

[49] Sun, H. *Eur. Phys. J. C* **2014**, *74*, 2977.

[50] Fichet, S.; von Gersdorff, G.; Kepka, O.; Lenzi, B.; Royon, C.; Saimpert, M. *Phys. Rev. D* **2014**, *89*, 114004.

[51] Fichet, S.; von Gersdorff, G. *J. High Energy Phys.* **2014**, *03*, 102.

[52] Senol, A.; Köksal, M. *Phys. Lett. B* **2015**, *742*, 143-148.

[53] Fichet, S.; von Gersdorff, G.; Lenzi, B.; Royon, C.; Saimpert, M. *J. High Energy Phys.* **2015**, *02*, 165.

[54] Fichet, S.; von Gersdorff, G.; Royon, C. *Phys. Rev. Lett.* **2016**, *116*, 231801.

[55] Köksal, M.; Arı, V.; Senol, A. *Adv. High Energy Phys.* **2016**, *2016*, 8672391.

[56] Selcin, G. A.; Şahin, İ. *Chin. J. Phys.* **2017**, *55*, 2305-2317.

[57] Billur, A. A.; Köksal, M.; Gutiérrez-Rodríguez, A. *Phys. Rev. D* **2017**, *96*, 056007.

[58] Arı, V.; Billur, A. A.; İnan, S. C.; Köksal, M. *Nucl. Phys. B* **2016**, *906*, 211-230.

[59] Altschul, B.; Bailey, Q. G.; Kostelecky, V. A. *Phys. Rev. D* **2010**, *81*, 065028.

[60] Carlson, D. O. PhD, Michigan State University, East Lansing, MI, USA, 1995.

[61] Martin, A. D.; Stirling, W. J.; Thorne, R. S.; Watt, G. *Phys. Lett. B* **2007**, *652*, 292-299.

[62] Piotrzkowski, K. *Phys. Rev. D* **2001**, *63*, 071502.

[63] Budnev, V. M.; Ginzburg, I. F.; Meledin, G. V.; Serbo, V. G. *Phys. Rep.* **1975**, *15*, 181-282.

[64] Baur, G.; Hencken, K.; Trautmann, D.; Sadovsky, S.; Kharlov, Y. *Phys. Rep.* **2002**, *364*, 359-450.